# Environmental Science Nano



# **PAPER**

View Article Online
View Journal



Cite this: DOI: 10.1039/d3en00306j

# Modifying soluble NPK release with hydrophobized nanocellulose-based hydrogels for sustainable enhanced efficiency fertilizers†

Diego Gomez-Maldonado, (1) ‡<sup>a</sup> Savannah G. Phillips, (1) ‡<sup>b</sup> Shital R. Vaidya, (1) c Paul C. Bartley III, d Jason C. White, (1) c D. Howard Fairbrother (1) b and Maria S. Peresin (1) \*a

Enhancing the delivery efficiency of NPK fertilizers benefits both crops and the environment through moderating the supplied dosage of nutrients in the soil, avoiding side reactions, maximizing absorption by the plant, and minimizing leaching and runoff. Bio-based materials such as cellulose are ideal scaffolds for nutrient delivery due to their inherent biocompatibility, biodegradability, and significant water uptake. In this work, nanocellulose-based hydrogels were regenerated from mixed softwood in acidic media and loaded with NPK by immersion in varied concentrations of an NPK-rich fertilizer solution. High loading of NPK was achieved within the hydrogel, but immersion in the matrix provided only slight slowing of nutrient release compared to rapid solubility of conventional formulations. Densification, crosslinking, and coating of the hydrogels with beeswax were ineffective strategies to further slow NPK release. Following these results, both gas and solution-phase esterification reactions of the cellulosic matrix with hexanoyl chloride were performed after NPK loading to introduce a hydrophobic surface layer. While solution-phase modification led to phosphorus leaching and was overall ineffective in altering nutrient release, the gas-phase modification slowed the release of P and K by more than an order of magnitude. Moreover, it was found that varying both the properties of the hydrophobic surface layer and the nutrient loading provide a means to tune release rates. Overall, this work demonstrates the potential of nanocellulose-based hydrogels to be used as an environmentally safe and sustainable vehicle for the controlled release of nutrients in agricultural applications.

Received 16th May 2023, Accepted 4th August 2023

DOI: 10.1039/d3en00306j

rsc.li/es-nano

#### **Environmental significance**

Systematic overapplication of fertilizers, due to a general inability to control nutrient release kinetics, causes runoff, leaching, and eutrophication which harm vulnerable ecosystems in addition to wasting resources. Although slow-release fertilizers that mitigate these outcomes have been developed using synthetic polymers, they are typically not tunable, biocompatible, or biodegradable. To address these issues and make use of an earth-abundant natural resource, a nanocellulose-based controlled release enhanced efficiency fertilizer (EEF) has been developed which allows for multiple unrefined feedstocks, with great potential for reducing the environmental impacts of using nanocellulose. Here, the release profile of NPK is modified by facile chemical modification of nanocellulose prills, highlighting the promise of such systems to slow the release of agrochemicals and tune release kinetics.

# Introduction

By the year 2050, the global population is predicted to exceed 9 billion people, making maintaining global food security one of the most significant challenges facing society. Fertilization is a crucial agricultural step as it allows for maintenance of soil fertility, thereby increasing yields and improving quality of crops. In turn, these improvements have allowed for population growth and economic development globally. One major agricultural challenge is the significant inefficiency of current agrochemical delivery. Currently, the efficiency of delivery and uptake of many agrochemicals is as

<sup>&</sup>lt;sup>a</sup> Sustainable Bio-Based Materials Lab, Forest Products Development Center, College of Forestry, Wildlife and Environment, Auburn University, 602 Duncan Drive, Auburn, AL 36849, USA. E-mail: soledad.peresin@auburn.edu

<sup>&</sup>lt;sup>b</sup> Department of Chemistry, Johns Hopkins University, 3400 N Charles St, Baltimore, MD 21218, USA

 $<sup>^</sup>c$  The Connecticut Agricultural Experiment Station, 123 Huntington Street, New Haven, CT 06511, USA

<sup>&</sup>lt;sup>d</sup> Department of Horticulture, College of Agriculture, Auburn University, Auburn, AL 36849, USA

 $<sup>\</sup>dagger$  Electronic supplementary information (ESI) available. See DOI:  ${\bf https://doi.org/10.1039/d3en00306j}$ 

<sup>‡</sup> Co-first authors.

low as 10-20%,3 which necessitates application of large amounts of agrochemicals as well as continuous reapplication. This overuse of fertilizers, in addition to varied nutrient requirements by crop and throughout the growth cycle, increases nutrient loss through volatilization, fixation, precipitation, and leaching of nutrients from the soil into the environment.<sup>2,4</sup> These losses provoke eutrophication in lakes and other estuarine ecosystems, while volatilization of nutrients leads to accumulation of greenhouse gases such as ammonia and nitrous oxide.5,6 Collectively, improper and inefficient fertilization strategies affect both environmental quality and quality of life. These pressures necessitate the development of more ecofriendly and efficient fertilizers.<sup>5,7</sup>

To mitigate fertilizer-induced pollution, new systems have been developed which control the release of nutrients.8 Such systems are commonly called enhanced efficiency fertilizers, or EEFs. 7,9 These fertilizers aim to contain the nutrients in some manner and reduce their dissolution rates into the environment. There are multiple approaches to achieve this; the first involves coating conventional fertilizer materials, such as urea, with hydrophobic polymers to reduce solubility.10 The second approach utilizes materials that are inherently slow to solubilize in aqueous systems, such as urea-aldehyde condensates. 11 A third, less-explored approach involves using water-soluble polymers as either coatings or carrier matrices for these nutrients.8 These polymers can be further modified by surface densification, crosslinking, and the addition of ligands to reduce the number of hydrophilic active sites. 12,13

Most applied fertilizers are underutilized by plants, as losses are common due to side processes. 10,14 Specifically, NPK-based fertilizers are commonly water soluble, which results in rapid nutrient leaching with precipitation and irrigation. Thus, increasing the hydrophobicity of such fertilizers with coatings allows for longer residence times in soils, minimizing the need for reapplication. In this way, EEFs have proven effective in reducing both the amount of fertilizer needed and the burden of continuous reapplication as retention times in soil are increased. 15 Nevertheless, most common EEF materials still generate environmental pollutants as byproducts.16 For example, many conventional coating methods utilize fossil-based materials, like polyethylene, to increase hydrophobicity and soil retention time.<sup>17</sup> Once the polymer degrades and the fertilizer is released, the residual polyethylene will remain in the environment and generate microplastics. 17,18 Moreover, in 2020 the worldwide demand for NPK fertilizers was 194.8 million metric tons (Mt), 19 with around 5% of those fertilizers being composed of microplasticgenerating materials.<sup>17</sup> Thus, NPK fertilization introduced 9.74 Mt of material to the environment in that year alone which will ultimately degrade into microplastics. Further, experts estimate that the annual requirement for NPK fertilizers will rise above 324 Mt by the year 2050,<sup>20</sup> with the potential to result in the release of 16.2 Mt of microplastics annually.

To avoid release and accumulation of microplastics in soil and aqueous environments, there is a clear need to explore environmentally-friendly biopolymer alternatives. Looking among sustainable biopolymers, cellulose is an intuitive candidate due to its ubiquity, known extraction and separation processes, and well-established global market. Additionally, there are many well understood processing methods for cellulose that allow control over its structural form. These processing methods enable formation of coatings, 21 films, 22 gels, 23 or foams. 24 This versatility enables selection of the form best suited to carry, retain, and release NPK fertilizers.

Most commonly, researchers have found that microparticulate hydrogel beads are ideal for releasing active ingredients as this geometry allows for a superior diffusion profile in both loading and release steps. Additionally, spherical-shaped particles promote intermediate processing steps, such as mixing and drying, which facilitate their large scale production.<sup>25–28</sup> These beads can be regenerated from natural cellulose sources through solubilization in cold alkaline sodium hydroxide and urea solutions followed by formation in acidic media. 29,30 This method has been shown to produce low density nanocellulose-based beads with a high water content that can be exchanged with other solutions, thereby trapping the molecules within the cellulosic matrix.31 These superabsorbent hydrogel beads have been explored as packaging materials, 29,32 drug carriers, 30,33 antimicrobial and water treatment scaffolds, 34,35 and cell carriers.<sup>36</sup> For the majority of these applications, the regenerated beads must be further washed to remove residual urea, nitrates, and nitric acid. However, in utilizing this processing method to encapsulate NPK fertilizers, these residues could act as an additional nitrogen source, removing the need for additional washing steps in the manufacturing process.

In addition to the application of coatings and chemical transformations such as cross-linking, the glucose subunits of cellulosic particles can be modified in multiple ways by reactions involving the hydroxyl groups. 37,38 Several new chemistries can be introduced in this way, including sulfates, carbonyls, silanes, alkynes, and aldehydes, as well as cationic and anionic groups. 37-39 Most often, these modifications introduce hydrophobicity, as they replace the hydrophilic hydroxyl groups with more hydrophobic moieties. 40 In extended release applications, these kinds of hydrophobic modifications have been shown to alter release in a controllable manner. For example, esterification of chitosanbased hydrogels with long chain fatty acids extends the release of acetaminophen. Moreover, the release rates were slowed as the extent of chitosan modification increased.<sup>41</sup> Similarly, an acetate-modified cellulose matrix extended the release of thymol over the course of days, with release kinetics dependent on loading of the analyte cargo and the media into which it was released.42 These effects are explained by changes to the pore structure and the crystallinity of the modified products.

There is a strong need to develop EEFs with tunable release kinetics constructed from naturally occurring, and sustainable materials. Motivated by this need, this work explores nanocellulose-based hydrogels as a carrier for NPK fertilizers. To further modify the cellulose matrix, crosslinking and coating methods were evaluated in addition to esterification in gaseous and solution phases. The EEF capacity of these materials was evaluated by aqueous release and monitored by Inductively Coupled Plasma Optical Emission Spectroscopy (ICP-OES).

# Materials and methods

#### **Materials**

Bleached cellulose nanofibrils (2.76 wt%, pH 6.3) (CNFs) were produced at the Sustainable Bio-Based Materials Lab at Auburn University from bleached pulp generated from mixed softwood, provided by a North American papermill. A soluble fertilizer (20, 20, 20, Nutriculture) was purchased from Plant Marvel (Chicago Heights, Illinois, US) and used as received. The safety data sheet provides the following concentration ranges for the fertilizer composition: 26-32% potassium nitrate, 26-32% urea, 15-20% monoammonium phosphate, 15-20% monopotassium phosphate. Nitric acid (ACS reagent grade) was purchased from Pharmco-Aaper (Mississauga, Ontario, Canada). Crystalized urea and acetone (99.5% purity) were purchased from VWR (Radnor, Pennsylvania, US). NaOH pearls (97% purity) were purchased from Alfa Aesar (Ward Hill, Massachusetts, US). Beeswax (bleached), maleic anhydride, and hexanoyl chloride (97% purity) were purchased from Sigma Aldrich (St. Louis, Missouri, US) and used as received. Unless specified, all weight measurements in this paper are expressed on an oven-dry basis.

#### Preparation of cellulose nanofibrils

Cellulose nanofibrils (CNFs) were prepared as described previously. Briefly, a cellulose pulp suspension was prepared at 2 wt% and washed with consecutive acidic and alkaline steps to eliminate the residual impurities of the pulping process. Thereafter, the pulp was neutralized and processed in a Masuko Super Mass Colloider (MKZA-10-15J) with 20 passes. The resulting suspension had a 2.8 wt% consistency from triplicate gravimetry measurements; pH was similarly measured in triplicate with a consistent value of 6.3.

#### Formation of the nanocellulose-based hydrogel beads

The formation of the hydrogel beads was done by adapting the process previously described.  $^{31}$  In brief, the produced suspension was diluted to 1.4 wt%. Sodium hydroxide (12 wt%) and urea (7 wt%) were then added to the solution while the temperature was lowered to  $-10\,^{\circ}\text{C}$ . Once homogenized, the solution was added dropwise (roughly 83  $\mu\text{L}$  with a 22 g needle  $^{44}$ ) into a volumetric cylinder containing 35 mL of a 2 M nitric acid solution and left to coagulate for 10 min. For washing of control samples, the residues remaining inside

the bead were eliminated through multiple solvent exchanges with ultrapure water using a 50  $\mu m$  cell strainer (VWR). This process was repeated until conductivity values matched those for pure water.

# Loading of the hydrogel beads with NPK fertilizer

Two methods for saturation were tested. First, pre-formed hydrogel beads (around 500 mg) were placed into 10 mL aliquots containing either 18 or 36 wt% NPK solution and left to soak for 72 hours for complete saturation. As the solubility of NPK salts can be increased by increasing solution temperature, a super-saturated solution was prepared by using 36 g of fertilizer added to 50 mL of ultrapure water at 75 °C, which was left stirring softly until solubilized. Then, 2.5 g of hydrogel beads were immersed into the hot solution and the temperature and stirring conditions were maintained for 2 hours. Once loaded, the hydrogel beads were dried in a convection oven at 35 °C overnight.

#### **Modification strategies**

Spray coating with beeswax. To form a waxy surface layer, a 2 wt% solution of beeswax in acetone was prepared and sprayed onto dried NPK-embedded beads using an airbrush (MP2900, Campbell Hausfeld). The beads were placed inside a centrifuge tube, covered with a 0.45  $\mu m$  mesh, and inverted for spraying. The tube was agitated continuously while spraying for 1 minute through the mesh. The tubes were then left open to allow residual acetone to dry.

Densification with maleic anhydride. An adapted densification method was used based on previous reports. <sup>45</sup> Briefly, dried CNF hydrogel beads were baked at 80 °C in a hermetic forced convection oven. The dry beads were first scattered on an aluminum tray (12 cm diameter, VWR). A smaller crinkled aluminum tray (1.3 mm) containing 2 mg of maleic anhydride and a few drops of HCl was then added to the larger tray. After 2 hours, the temperature was increased to 120 °C and the reaction allowed to proceed for 30 minutes at this elevated temperature.

Gas-phase esterification. To introduce hydrophobic groups to the CNF beads, gas phase esterification was performed.<sup>46</sup> Fig. 1 shows the modification to the monomeric structure upon esterification.

Briefly, 0.5 mL of hexanoyl chloride was added to the bottom of a custom-designed Schlenk line vessel, and 75 mg of NPK-CNFs were loaded into a separate suspended

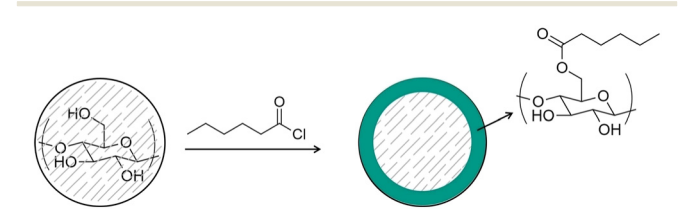


Fig. 1 A reaction scheme showing modification of a nanocellulose hydrogel, resulting in formation of an esterified, hydrophobic shell.

compartment (see Fig. S1† for a graphic of the customdesigned vessel). The bottom of the vessel was then submerged in liquid nitrogen to quickly freeze the hexanoyl chloride, followed by brief evacuation of the vessel for approximately a minute to achieve a low pressure between 10 and 50 mTorr. The vessel was then sealed to allow the hexanoyl chloride to warm and sublimate, esterifying the surface hydroxyl groups on the CNF bead over time as shown in Fig. 1. To stop the reaction after the desired time, the vessel was re-opened to air. The esterified NPK-CNFs were then placed in a new vessel without hexanoyl chloride and evacuated to remove any remaining unreacted reagent.

**Solution-phase** esterification. As an alternative esterification strategy, NPK-loaded CNF beads were also esterified in solution. Briefly, 75 mg of NPK-CNFs were submerged in 5 mL of hexanoyl chloride in a 10 mL beaker. The beads were allowed to sit in solution for 72 hours before filtering to remove excess hexanoyl chloride. The beads were washed 3 times with approximately 20 mL of diethyl ether before leaving to dry at room temperature for at least 24 hours.

#### Characterization techniques

Dry content. The nanocellulose-based hydrogel beads were weighed before and after NPK loading in aluminum pans (masswet) and dried in an oven at varied temperatures to remove moisture and allow the dry mass (mass<sub>dry</sub>) to be determined. The unloaded hydrogels were dried at 105 °C, densified beads were baked at 80 °C, and NPK-embedded beads were dried at 35 °C. The moisture content (MC) was calculated according to eqn (1).

$$MC\% = \frac{mass_{wet} - mass_{dry}}{mass_{wet}} \times 100\% \tag{1}$$

All measurements were performed in triplicate, and an average value was calculated. The percentage of solid content was determined as the difference between the total mass (100%) and MC%. Meanwhile, the amount of fertilizer present was calculated by the difference between the dry mass obtained without the salts and the dry mass obtained in the presence of the salts.

Attenuated Total Reflectance-Fourier Transform Infrared **Spectroscopy** (ATR-FTIR). The dried samples were analyzed using a Nicolet iS5 FT-IR spectrometer with a Thermo Fisher iD5 ATR accessory using a diamond crystal. The spectra were collected with 32 scans and 2 cm<sup>-1</sup> of resolution. Baseline correction was performed using OMNIC software, and normalization was performed manually using Excel.

Scanning Electron Microscopy (SEM). Freeze-dried samples were placed onto aluminum studs before being sputtered with gold in an EMS 550X Sputter Coating Device from Science Services (Munich, Germany). After coating, the samples were imaged in a Zeiss Evo 50VP scanning electron microscope (Oberkochen, Germany).

X-Ray Photoelectron Spectroscopy (XPS). To characterize the bead surfaces, survey and detailed XPS spectra were collected with a PHI 5600 XPS using a Mg Ka flood source (1253.6 eV photon energy) at a 54° take-off angle. Survey spectra were taken at a pass energy of 187.85 eV with a resolution of 1.6 eV per step with 5 sweeps per spectrum. Detailed scans of the C 1s/K 2p, O 1s, N 1s, and P 2p regions were taken for all samples at a pass energy of 23.5 eV, 0.025 eV per step resolution, and 10 sweeps per spectrum. Elemental compositions were determined using CASA XPS software and converted to weight percentages using Excel.

Elemental Analysis (EA). To obtain chemical information on the bulk composition of the beads, CNF samples embedded with varied loadings of NPK fertilizer were sent to Midwest Microlab (Indianapolis, IN) for elemental analysis. All samples were analyzed for CHN (carbon, hydrogen, and nitrogen) as well as phosphorus. Oxygen content could not be determined for these samples due to interferences from phosphorus, and potassium content cannot be measured by

#### Timed release testing of phosphorus and potassium in water

The release of P and K from esterified and unmodified NPKloaded CNF beads were analyzed by ICP-OES (Thermo Scientific, iCAP 6000 series spectrometer) to determine elemental phosphorus and potassium. The ICP-OES was calibrated with the method blank of 2% nitric acid and 0.1 ppm, 1 ppm, and 10 ppm standard solutions (quality control standard 7 and 21, SPEX CertiPrep, Metuchen, NJ, USA). Ten ppm yttrium was used as an internal standard. Calibration verification was maintained throughout analysis after every 15 samples. While ICP-OES is not equipped to detect nitrogen due to weak emission lines, previous studies have shown that the release of various nitrogen-containing nutrients follow closely with the release of potassium and phosphorus-containing nutrients. 47,48

For release experiments, 19 mg of NPK-loaded beads were placed in 20 mL of MilliQ water. Aliquots of water (2 mL) were taken from these solutions at specific times and diluted to 5 mL with MilliQ water. Immediately following the removal of these 2 mL aliquots, a 2 mL aliquot of MilliQ water was added to maintain a constant volume. This procedure was repeated for all timepoints. Each sample was then acidified (5%) with 70% nitric acid and subsequently analyzed for P and K content by ICP-OES. All P and K concentrations were adjusted to reflect the dilution that occurred between subsequent samples, with each sequential sample having a dilution factor of 20/18 to account for the addition of 2 mL of MilliQ water. All control samples were released in triplicate; however, due to low sample availability, replicates were not taken for modified samples. Throughout the release, the hydrogel beads sink in water, such that no beads are taken up during aliquot collection and the bead remains submerged throughout the release profile. Since all of the nutrients were found to release over the relevant experimental timescales (SEM-EDS data shown in the ESI†), raw data in mg L-1 could be converted to percentage of

nutrient released based on the observed maximum concentrations for P and K per sample.

# Results and discussion

#### Formation of cellulose hydrogel beads and loading capacity

The cellulosic hydrogel beads were found to have a solid content of  $2.2 \pm 0.4\%$  and a size of  $2.8 \pm 0.2$  mm, similar to other reported studies. The low solid content in the beads suggests that when highly ionic NPK solutions are exchanged for the liquid inside, the driving mechanism will be the osmotic pressure, with the absorption and water retention in the bead structure resulting from the ionic nature of the salts contained in the fertilizer media. As such, a soluble salt-based fertilizer will be the ideal cargo to be carried by these cellulosic hydrogels.

To assess the loading capacity of the hydrogels (Fig. S1†), completely washed beads were placed into saturated solutions of the soluble NPK fertilizer and allowed to sorb for 72 hours before the solution was diluted to concentrations between 10 and 360 g L<sup>-1</sup>. As a function of NPK concentration, the increase in adsorption capacity (as determined by the bead's mass gain) was roughly linear, with two distinct slopes observed. At relatively low fertilizer concentrations (less than 100 mg L<sup>-1</sup>), a relatively modest increase in adsorption capacity was observed and is attributed to adsorption of the fertilizer ions and salts to the surface of the exposed nanocellulose. At higher fertilizer concentrations, the second slope is guided by a more rapid increase in adsorption capacity which likely corresponds to the absorption of the ions into the interior of the hydrogel.

After these initial studies to estimate loading capacity, any further washing of the beads was avoided to ensure retention of the residual nitrogen-containing compounds which serve as an additional source of nitrogen. Without washing, it was observed that over 71 wt% of the dry unwashed solid content of the beads was composed of these urea and nitric acid

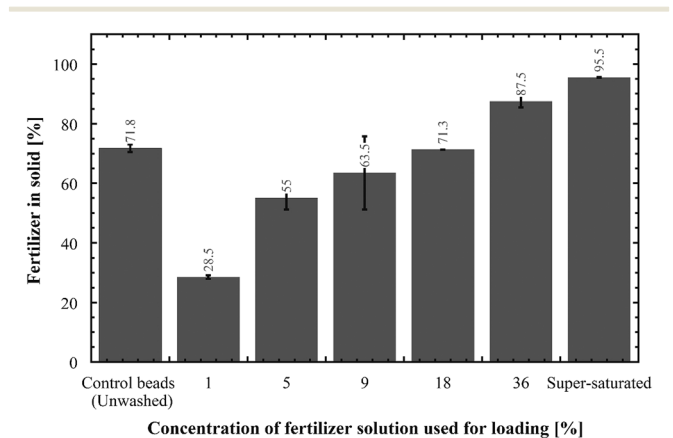


Fig. 2 Percentage of (oven-dried) bead's total dry weight comprised

of fertilizer: unwashed beads (containing residual nitrates and urea) and beads that were loaded by immersion into solutions with different fertilizer concentrations (1, 5, 9, 18, 36 wt%) and a super-saturated solution (72 wt% at 75 °C).

residues. When these unwashed beads were placed into solutions of the solubilized NPK fertilizer, the solid of fertilizer decreased at lower concentrations (Fig. 2, Table S1†). The rationale for this behavior lies in relative concentration of ions embedded inside the beads compared to the ion concentration in the solution. As has been observed previously, the concentration of ions determines the mass flow. 49 Since the urea and sodium concentrations in the cellulose solution were 7 and 12 wt%, respectively, the beads immersed in NPK solutions below 18% lost some of the solids that were initially retained. For higher concentrations of NPK, including the supersaturated solution, the mass flow favors ion incorporation of NPK into the beads and as a result the percentage fertilizer loaded is competitive with concentrations found in other commercial coated EEFs.17

To better understand the changes that occurred upon bead formation and loading of the NPK, ATR-FTIR spectra were obtained of fully washed beads (urea and nitrate eliminated), the unloaded unwashed control beads, and the 36% NPK-loaded control beads (Fig. 3).

As suspected, the fully washed beads present the spectrum of regenerated cellulose II in the absence of any other spectral features due to the mercerization process.51,52 In addition to the expected cellulose bands, the unwashed control beads display bands at 1624 and 1668 cm<sup>-1</sup>, supporting the significant increase in solid content associated with urea.53 Additional bands can be assigned to intermediate states of nitrocellulose, which are expected under nitrate-reducing conditions.<sup>54</sup> Specifically, the bands above 1600 cm<sup>-1</sup> and 800 cm<sup>-1</sup> correspond to residual nitrate from the nitric acid, while the weak bands between 2300 and 2400 cm<sup>-1</sup> correspond to background CO<sub>2</sub> asymmetric stretching.55 Once these unwashed control beads were loaded with NPK fertilizers, a broadening of the N-H and O-H bands was observed, as well as the appearance of broad bands between 1300-1450 cm<sup>-1</sup> and 1500-1700 cm<sup>-1</sup>. These

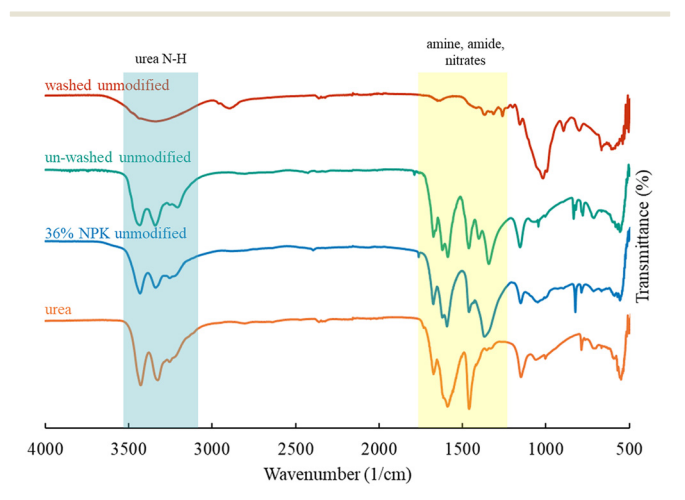


Fig. 3 ATR-FTIR spectra for unloaded, washed (nitrate and urea eliminated) control beads, unloaded control beads, 36% NPK-loaded control beads, and urea. Areas of interest are shaded.

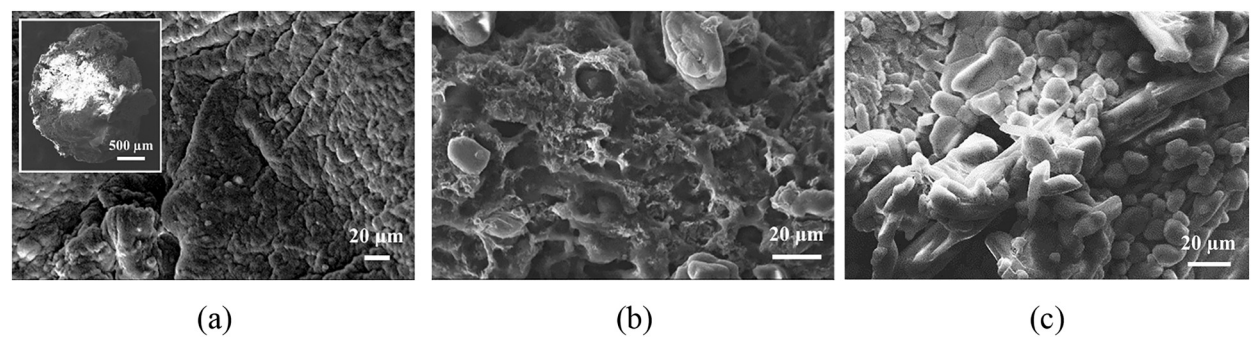


Fig. 4 SEM images of control, unmodified CNFs: (a) washed control bead with insert showing a whole dry bead with an approximate size of 1 mm (the scale bar for the insert is  $500 \mu m$ ), (b) unwashed control, and (c) 36% NPK-loaded control bead.

bands correspond to the amines and nitrates contained in the commercial fertilizer.

SEM images were obtained to determine the morphological changes in the beads caused by the introduction of the urea and the NPK salts (Fig. 4). These revealed that the washed control beads were approximately spherical with a radius of several hundred microns and exhibited a smooth surface with clear hornification of the cellulosic fibers (insert to Fig. 4a). The unloaded and unmodified control bead (Fig. 4b) presented crystals on the surface that can be linked to the residual urea and alkali from the dissolving process. Likewise, the surface had more rugosity as the fibers were not able to conglomerate freely. SEM also shows clear crystals on the surface of the NPK loaded CNF beads with several protuberances created by salt recrystallization.

To better understand the distribution of NPK fertilizer components throughout the bead, a combination of surface-sensitive XPS and bulk elemental analysis was used. Fig. 5, below, shows detailed XPS scans of the O 1s, N 1s, K 2p, C 1s, and P 2p regions for all loading percentages of NPK. Survey scans from 0 to 1100 eV can be found in the ESI† (Fig. S7).

For comparison, the C, H, N, and P elemental analysis for the same set of samples are shown below in Table 1, compared with the surface-sensitive values determined by XPS.

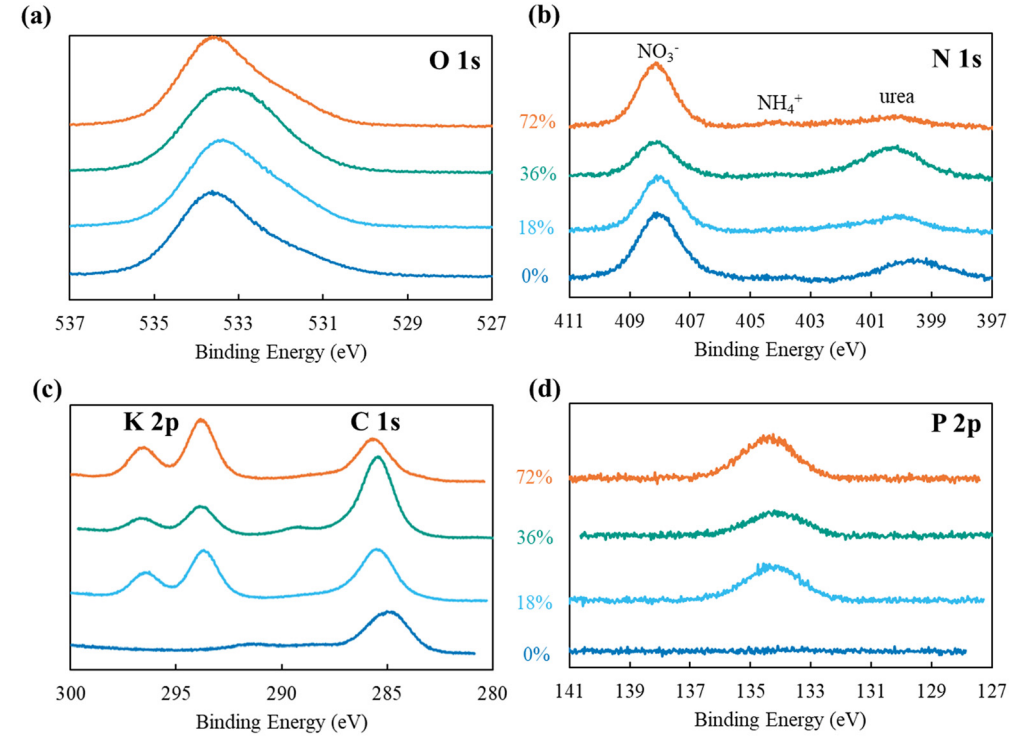


Fig. 5 Detailed XPS scans of variously-loaded NPK-CNFs: a) O 1s, b) N 1s, c) K 2p and C 1s, and d) P 2p regions. Spectra were normalized based on the intensity of the O 1s peak, and binding energies were calibrated based on the nitrate  $NO_3^-$  peak at 408.1 eV.<sup>56</sup>

Table 1 A comparison between the weight percentage of various elements at the surface of CNF beads (determined by XPS) and the overall elemental composition of the beads (determined by elemental analysis). It should be noted that the measurement of oxygen by elemental analysis was not possible due to phosphorus interference

	Surface (XPS)					Overall (elemental analysis)			
Sample	C (wt%)	O (wt%)	N (wt%)	P (wt%)	K (wt%)	C (wt%)	H (wt%)	N (wt%)	P (wt%)
0%	36.7	40.0	11.7	0.43	0.0	18.7	3.9	19.2	0.0
18%	30.7	37.0	8.5	3.8	18.8	17.4	4.3	14.9	10.9
36%	39.1	31.3	8.2	2.6	9.2	12.5	3.7	19.8	27.0
72%	24.1	35.8	9.6	4.8	24.7	15.7	4.1	15.2	12.0

Comparing these XPS and EA results provides insights into the nutrient distribution throughout the beads. Despite the inability to compare the levels of oxygen at the surface to the overall oxygen content, there is a significantly higher percentage of carbon at the bead surface than would be anticipated on the basis of the bead's overall chemical composition. Since the carbon atoms are primarily associated with the cellulosic backbone, this distribution indicates that there is certainly no preference for NPK accumulation at the surface and suggests a preference for NPK encapsulation within the beads. This assertion is also supported by the smaller nitrogen and potassium concentrations at the surface than would have been expected on the basis of overall composition (Table 1).

Looking to the XPS data for surface characterization, the higher amount of nitrogen present in the unloaded (0%) beads relative to any of the NPK-loaded samples supports the presence of crystalline urea on the bead surface, corroborated by SEM images (Fig. 4b). Amongst the NPK-loaded samples, the nutrient concentrations show the expected increase moving from 18 to 72% loading, assuming that the overall potassium loading follows the trends of nitrogen and phosphorus. However, the lowest concentrations of NPK components at the surface are observed at 36% loading; conversely, the 36% sample has the highest bulk concentration of nitrogen and potassium. These higher bulk and lower surface nutrient concentrations observed for 36% loaded NPK-CNFs suggest superior nutrient encapsulation at this loading percentage, when compared with 18 and 72% loading. More generally, these results suggest that the relative distribution of NPK nutrients at the surface compared to the interior may be sensitive to nutrient loading.

## **Esterification of NPK-CNF beads**

ATR-FTIR spectra were also collected for CNF-based beads after gas phase esterification with hexanoyl chloride at each NPK loading percentage. Fig. 6 shows the 36% NPK-CNFs after esterification; ATR spectra for the other NPK loadings can be found in the ESI† (Fig. S3).

Compared with the unmodified cellulosic hydrogels, the functionalized particles show some additional bands superimposed on those associated with NPK nutrients and residual urea. For example, there is a notable increase in the C–H stretching region (2800–3000 cm<sup>-1</sup>), consistent with the

addition of the alkyl chain associated with the esterification process (see Fig. 1). Esterification is also suggested by the increased intensity of bands in the 1600–1700 cm<sup>-1</sup> region, representing the introduction of carbonyl species. In addition to other new bands in the fingerprint region, all these spectral changes to the IR are consistent with modifications to the cellulose backbone expected from esterification, as shown in Fig. 1, although more detailed analysis is made difficult by the broad spectral features associated with the NPK nutrients and residual urea.

SEM images (Fig. 7) indicate that when unloaded beads were esterified, large crystals were formed on the bead exterior, indicating an additional sedimented layer of hydrophobicity produced on the surfaces due to saturation after the gas phase deposition. This new crystalline layer was also observed in the NPK-loaded and esterified sample; however, the more crystal-like structures created by NPK salts were retained upon esterification and expanded, suggesting that the new esterified layer was formed homogenously on the surface.

#### Characterization of materials after release

ATR-FTIR spectra were collected for unmodified and modified NPK-CNFs after all nutrients had been released

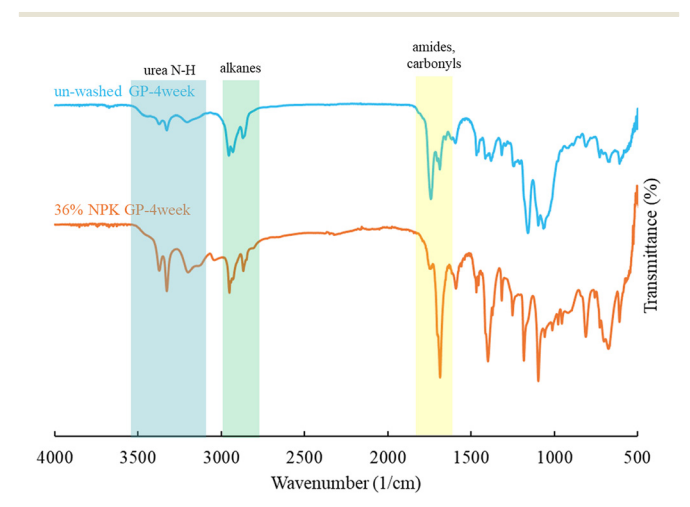


**Fig. 6** ATR-FTIR spectra of gas-phase (GP) modified (reacted for 4 weeks) CNF beads: unloaded and unwashed (top) and 36% NPK-CNF beads (bottom), plotted in terms of transmittance. Areas of interest are shaded.

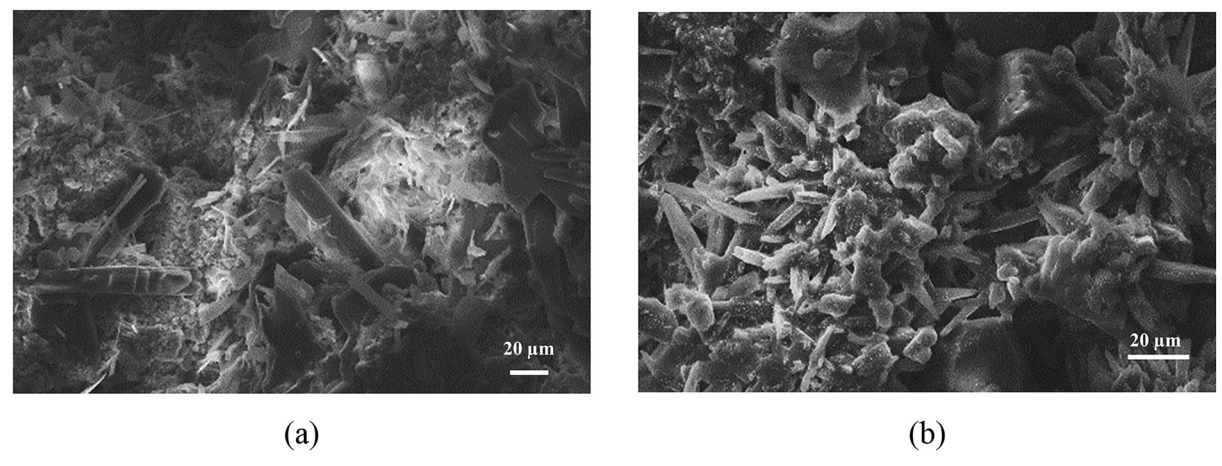


Fig. 7 SEM images of the gas-phase esterified CNF beads: (a) unwashed 0% and (b) 36% NPK-loaded.

through immersion in water, and the residual solid material was extracted by subsequent freeze-drying. These spectra are shown below in Fig. 8 for 36% NPK-CNFs. ATR-FTIR spectra for CNFs initially loaded with different NPK percentages can be found in the ESI† (Fig. S8).

Following removal of NPK bands as a consequence of their release, the nanocellulose matrix structure can be clearly discerned with broad N-H and O-H stretching bands from 3600-3100 cm<sup>-1</sup>, C-H sp<sup>2</sup> and sp<sup>3</sup> bands from 3000-2850 cm<sup>-1</sup>, and characteristic broad C-O stretches from 1200-1000 cm<sup>-1</sup>.<sup>57</sup> The small band at 1650 cm<sup>-1</sup> can be attributed to adsorbed water, commonly observed in cellulose and similar materials. In contrast, CNFs modified by esterification display a significant increase in C-H stretching that was visible in Fig. 6, in addition to the new carbonyl stretch associated with esterification now clearly evident at 1740 cm<sup>-1</sup>. This C=O band is distinct from that of hexanoyl chloride, which occurs at 1710 cm<sup>-1</sup>.58 The significant reduction in O-H stretching (3600-3100 cm<sup>-1</sup>) along with the intense C=O band indicate a high degree of esterification.

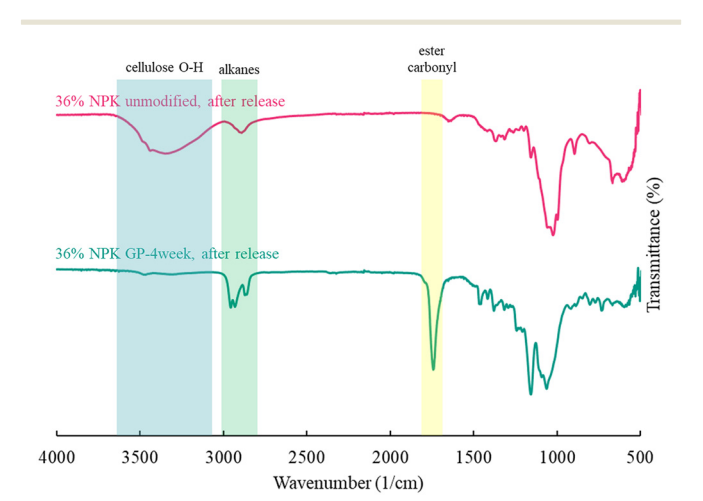


Fig. 8 ATR-FTIR spectra of unmodified and gas-phase (GP) hexanoylmodified NPK-CNFs at 36% NPK loading, after complete aqueous release of nutrients. Areas of interest are shaded.

The lack of any other spectral features in the modified NPK-CNFs after immersion in water provides strong support for the idea that all of the NPK nutrients have leached from the matrix and that functionalization (Fig. 1) does not cause any unwanted side reactions with the NPK that precludes their release.

SEM images (Fig. 9) show the gas-phase esterified unloaded and 36% NPK-loaded CNFs after release. For these samples, the surface looked similar to the modified control absent the excess crystal-like structures, which provides further confirmation that some of these crystals resulted from esterification. Larger porosity was also observed in the loaded beads, but no NPK salts can be seen, confirming the release of the NPK fertilizer.

### Phosphorus and potassium release kinetics and the influence of surface modification

Release tests were performed with the as-prepared loaded fertilizer beads before any modification using the change of water conductivity as the indicator of ion release. This method is described further in the ESI.† It was found that ion release was completed over the course of 30 minutes; absent of the nanocellulose matrix, these nutrients are soluble in water, resulting in immediate release. The slower release kinetics are most likely driven by the osmotic pressure of the cellulosic network that dictated the release profile of nutrients from the fertilizer beads.<sup>49</sup> Despite the relatively rapid release of ions from the unmodified CNF beads, a notable relative difference in release rates was observed depending on the initial concentration of NPK loading. Specifically, the beads immersed in the 36% NPK solution resulted in the slowest release (Fig. S10†).

CNF hydrogels after NPK release were also analyzed by SEM-EDS, to determine if residual nutrients remained (see ESI† for experimental details and Fig. S9† for results). These spectra support complete release of NPK from the hydrogel matrix, with only trace impurities present.

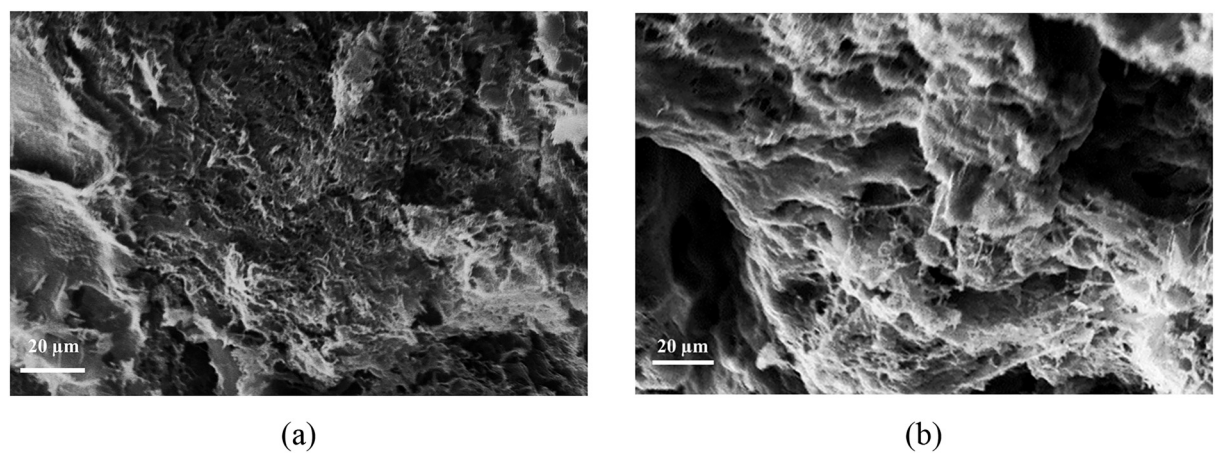


Fig. 9 SEM images of CNF hydrogels after release of nutrients: (a) GP-4week modified control and (b) GP-4week modified 36% NPK bead.

Unfortunately, the release profile was not sufficiently improved to be competitive with commercial coated urea, which can extend the release of fertilizers over several days to weeks. 10,14 Despite this, it should be noted that the method described herein of hydrogel formation and NPK saturation generates high loading of nutrients of up to 95.5 wt%, which will enable high localized delivery while minimizing the amount of nanocellulose matrix needed. Further, this method is unique in its retention of residual nitrogen from the bead formation media. This provides additional nitrogen sources to the plant, utilizing what might otherwise be considered a waste product as a fertilizer amendment. Indeed, these forms of residual nitrogen present in the bead (urea and nitrates), are bioavailable to plants, 59 and the loading of nitrogen is relatively high (71.8 wt%). As such, the unwashed hydrogels themselves even before NPK fertilizer is embedded could be treated as a nitrogen-only fertilizer or soil amendment. Since plants typically require more nitrogen than potassium and phosphorus,60 there is a need for such nitrogen-exclusive systems. Thus, this method has the potential to use residual contaminants, which would otherwise be disposed of, as a bioavailable form of nutrients.

To tune release, the CNF hydrogels were further modified by densification with maleic anhydride and coating with beeswax. ATR-FTIR spectra (Fig. S4†) and SEM images of the modified unloaded CNFs (Fig. S5†) and 36% NPK CNFs (Fig. S6†) were taken to corroborate the modifications. These spectra supported successful modification of the native cellulose structure as intended. Using the same conductivitybased approach for the unmodified CNFs, NPK release rates in water were measured by monitoring changes in conductivity in ultrapure water (see Fig. S11†). However,

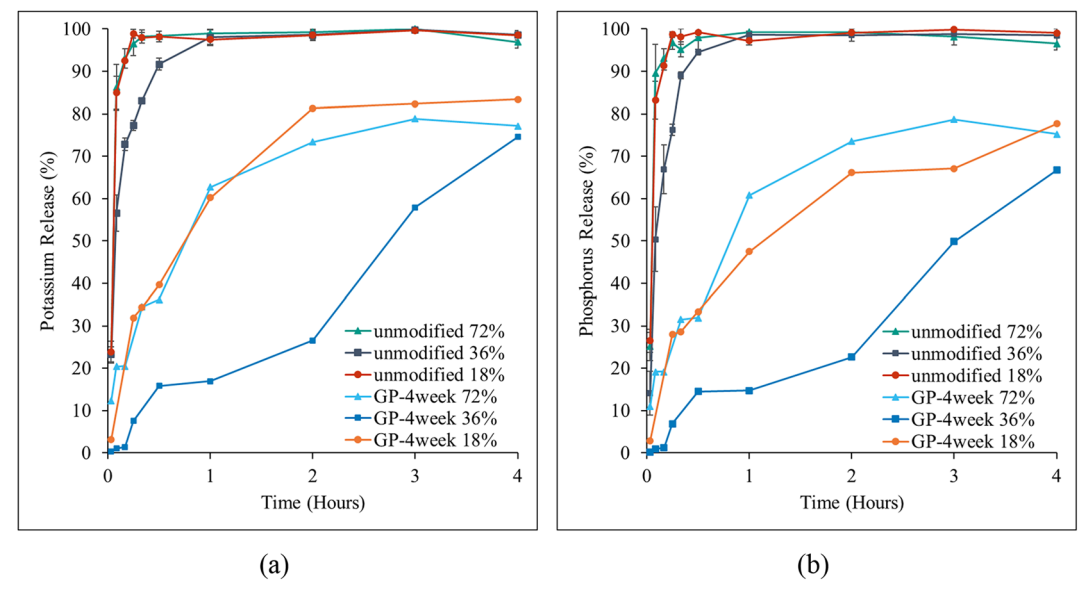


Fig. 10 Scaled ICP-OES data showing the release of potassium (left, a) and phosphorus (right, b), for unmodified and gas-phase modified (denoted GP) samples at loadings of 18, 36, and 72% NPK, plotted in terms of percent release, for the first 4 hours. Error bars are shown for all unmodified samples.

these results revealed that ion release was again complete after approximately 30 minutes for each of the modified CNFs, comparable to results obtained with hydrogels absent modification. Although these modifications resulted in extension of ion release of about 1 minute past the initial 30 minutes achieved with unmodified samples (Fig. S10†), this does not represent a significant improvement. As these modifications had minimal effect on nutrient release, it is likely that full surface coverage was not achieved, thereby leaving dissolution channels open for rapid nutrient release.

In another approach to slow the NPK release kinetics, CNF beads were passively esterified with hexanoyl chloride for 4 weeks. The potassium and phosphorus release profiles for unmodified and gas-phase (GP) esterified NPK-CNFs were determined by ICP-OES and are shown in Fig. 10. For esterified hydrogels, release measurements were taken for up to 72 hours, resulting in complete release of NPK from the matrix. Complete release profiles can be found in the ESI† (Fig. S12).

After esterification, the nutrient release rates decreased significantly, with the changes in phosphorus and potassium release kinetics mirroring one another. While the unesterified matrix released all nutrients within 30 minutes, the esterified samples had released between 16 and 40% of NPK by this time. This slowed release is likely a result of the introduction of a hydrophobic barrier at the microparticle surface, which prevents rapid dissolution of NPK from the interior.

In addition to the effect of the hydrophobic shell, the rate of nutrient release after esterification was also found to be somewhat dependent on the initial loading of NPK, analogous to the data obtained for unmodified CNFs. Fig. 10 shows that the initial release rates of the 72% and 18% NPK loaded CNFs were quite similar, with 75 and 78% of the phosphorus being released within 4 hours, respectively. As with the unmodified samples, the CNF beads loaded with 36% NPK fertilizer provided the slowest release of nutrients. After 4 hours, only 67% of the phosphorus had been released from the hydrogel matrix, with the remaining 33% of NPK releasing over the course of 72 hours (Fig. S12†). This timescale is competitive with other biopolymer-based controlled and slow-release systems; 61 however, it is not yet comparable with traditional polymer-based systems.

The slower release profile obtained from the 36% NPK-CNF beads was partially ascribed to these particles containing significant nutrient loading without having introduced significant osmotic pressure, which was seen at higher NPK loading. At 36%, loading remains well below saturation of the hydrogel, while still containing significant nutrients to be released over extended periods. Further, XPS and EA show that while 36% loaded NPK-CNFs contain the highest concentration of nutrients encapsulated within the bead, the 18 and 72% loaded samples contain more nutrients at the bead surface. Since nutrient release in this system can reasonably be assumed to be diffusion-controlled, release kinetics are expected to be slower for beads where nutrients

are preferentially encapsulated within the interior of the beads, as opposed to the exposed surfaces. Thus, the slower-release behavior observed at 36% loading can be rationalized, as 36% loading resulted in a greater fraction of nutrients being encapsulated within the beads when compared with the 18 and 72% samples (see Table 1). Moreover, the slower release profiles observed for the unmodified samples at 36% loading are retained after modification, which further supports that both loading and surface modification can be used to tune release rates.

Motivated by these promising initial results, further experiments were performed involving a longer reaction time (6 weeks) for nanocellulose esterification, which results in more extensive esterification. In experiments involving 6-week functionalized CNFs, only one loading percentage of NPK was used to control for this variable. The initial 4-hour release plots for the 6-week functionalized CNFs as measured by ICP-OES, are shown below in Fig. 11, compared with results from the unmodified and 4 week-esterified samples. Complete ICP-OES release plots, up to 72 hours, can be found in the ESI† (Fig. S13).

Analysis of Fig. 8 reveals that there is a discernible difference in release profile between the two esterified samples. Namely, the more-esterified sample, which was modified for 6 weeks, released potassium and phosphorus nutrients more quickly than the 4-week modified CNF sample, despite a higher degree of functionalization. This result counters the expectation that imparting a higher degree of hydrophobicity should provide the slowest release of soluble nutrients. One possible explanation for this observation is that esterification beyond a critical point results in a breakdown of the microbead structure, thereby creating channels for rapid nutrient dissolution. However, this counter intuitive dependence of release rates on degree of functionalization does suggest that lower levels of functionalization, which are easier to perform, may slow the extent of NPK dissolution further, providing even greater control over release rates.

After observing the extended-release profiles obtained with gas-phase modification, solution-phase modifications using hexanoyl chloride were also performed and the release of P and K was analyzed. It was found, however, that solutionphase modification led to selective leaching of phosphorus from the material, likely caused by contact between the CNFs and the liquid hexanoyl chloride or during subsequent washing with diethyl ether. Additionally, this modification did not result in any improvement in NPK release kinetics, compared with unmodified control samples. Further, only minimal esterification of the nanocellulose matrix occurred via this method as determined by ATR (data not shown). The obtained ICP-OES release plots can be found in the ESI† (Fig. S14). Given these results, solution-phase modification of the cellulosic beads is not a viable strategy for controlling release.

In addition to its ability to control release rates, gas-phase esterification has several notable benefits as compared to

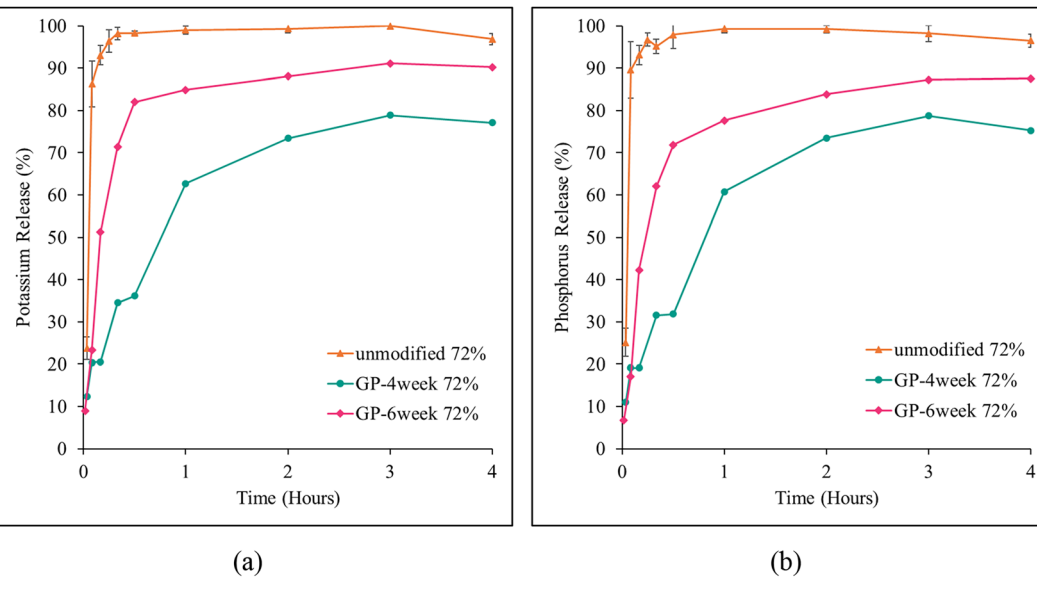


Fig. 11 ICP-OES release plots for potassium (left, a) and phosphorus (right, b) for 72% NPK-CNFs that were unmodified (triangles) and gas-phase (GP) esterified for 4 weeks (circles) and 6 weeks (diamonds), for the first 4 hours of release.

analogous solution-phase methods. Gas-phase modification requires no solvents during the reaction or in subsequent washing steps. This provides both cost savings and makes the reaction environmentally benign. Additionally, no pH adjustments or high temperatures are involved in this contrast modification, with conventional modifications. 62-66 Further, no energy input is required beyond the initial pulling of vacuum for less than a minute. The functionalization occurs passively over time, with minimal monitoring needed. This method is also easily scalable, only requiring a large enough glass manifold and sufficient pumping necessary to achieve a reduced pressure in the milliTorr range.

Further, since the reagent is in the gas phase, initial modification is known to occur at the hydrogel surface to create a hydrophobic core, hydrophilic shell structures. 67,68 Core-shell structures have been developed extensively to control delivery of varied active ingredients. 69-72 Surface properties play a crucial role in resultant material properties and in forming a hydrophobic barrier to water diffusion.73-75 Indeed, core-shell structures are ideal for environmental applications, as they minimize the extent of modification necessary to achieve the desired material properties through specific modification of the surface. Thus, using such a surface specific reaction minimizes the modification to the matrix required to achieve the desired change in material properties, namely, solubility and hydrophobicity. By retaining as much unmodified cellulose backbone as possible, this modification strategy retains much of the completely biocompatible and biodegradable cellulose, while the ester groups introduced as part of the functionalization are susceptible to enzyme hydrolysis. In contrast to hydrophobic modifications achieved through fluorination, esterification does not create any halogenated

products, which could produce toxic waste and cause environmental harm upon degradation. These observations highlight the sustainable nature of this gas phase modification strategy relative to other conventional solution-phase methods.

#### Kinetic analysis of P and K release

For quantitative characterization of relative release rates, a kinetic analysis was performed. It was found that the initial release profiles (up to 4 hours) could be reasonably well fitted to a first order exponential model as shown in eqn (2):

$$A_t = A_0 (1 - e^{-kt}) (2)$$

Here,  $A_t$  represents the concentration of P or K released from the nanocellulose matrix (in units of mg  $L^{-1}$ ) after time t (in hours),  $A_0$  indicates the final concentration of P or K solution upon complete release of the nutrient (mg  $L^{-1}$ ), k is the rate constant (in units of hour<sup>-1</sup>). Excel's Solver function was used to minimize the error squared values between experimental and kinetically derived concentrations. The resultant plots and fits can be found in the ESI† (Fig. S15 and S16). While more complex kinetic models for agrochemical release are reported in the literature, 78,79 this simple model provided an adequate fit and a quantitative means to assess the impact of hydrophobization on the release kinetics. Although this relationship does not provide any direct mechanistic insights into the release process, first order kinetic models have been used to describe drug and nutrient release from controlled delivery systems.80,81 Furthermore, it is well known that hydrophobic modifications can alter release of active ingredients from a matrix, 41,82,83 as these modifications alter solubility of bioactive compounds and delivery matrices in various media and other surface properties.84-87 The rate

Table 2 Derived rate constants for release of P and K from CNF hydrogels and average correlation coefficients for the release of phosphorus and potassium. Standard deviations are reported for control samples, wherein aqueous release was done in triplicate

Sample	Phosphorus rate constant (hour <sup>-1</sup> )	Potassium rate constant (hour <sup>-1</sup> )	$R^2$
Control 18%	$15.2 \pm 1.2$	15.3 ± 0.9	0.969
Control 36%	$6.8 \pm 1.9$	$7.5 \pm 1.2$	0.986
Control 72%	$16.4 \pm 0.6$	$15.4 \pm 1.3$	0.959
GP-4week 18%	0.759	0.937	0.968
GP-4week 36%	0.216	0.259	0.943
GP-4week 72%	0.671	0.823	0.954
GP-6week 72%	2.56	3.65	0.972

constants for phosphorus and potassium release for all of the control and gas phase (GP) modified CNF samples studied can be found in Table 2, along with adjusted correlation coefficients  $(R^2)$ , calculated in Excel. The correlation coefficients shown are the averages obtained across potassium and phosphorus.

Correlation coefficients for both potassium and phosphorus show good agreement between experimental data and the kinetic model, with all values being well above 0.9. Analysis of Table 1 reveals that the rate constants for the release of phosphorus and potassium from each sample occur at similar rates, with the slightly higher (averaging 25%) rate of potassium release attributed to the relative aqueous solubilities of these species.88 More importantly, the derived rate constants clearly show that modification decreased nutrient release rates by an order of magnitude or more for all NPK loading percentages, demonstrating the capacity for such modification to significantly slow release. This kinetic analysis confirms the tunability in rate constant made possible by controlling the reaction time and therefore extent of esterification, as evident by the approximately fourfold difference in phosphorus and potassium release rates between GP-6week and GP-4week samples.

These results also demonstrate that 36% loading capacity of NPK slowed release to the greatest extent when compared with 18% and 72% loading, for both modified and unmodified control samples. Specifically, for CNFs esterified for 4 weeks, 36%-loaded CNFs exhibited a threefold decrease in release rate compared to the modified 18% or 72% loaded CNFs. Moreover, the similarity in relative release rates between unmodified and modified CNFs indicates that release rates of active ingredients from CNFs is determined by a combination of the active ingredient loading and the degree of functionalization.

Compared with conventional controlled release fertilizers, such as coated urea, 10,14 the extended-release profiles shown herein are not yet functionally beneficial. While these less environmentally benign methods can extend release further than the results reported here, 10,14 the release profiles obtained upon hydrophobic modification of these CNF hydrogels can be compared with reported results for similar biopolymer-based controlled release systems. For example, spray-drying of chitosan/nanocellulose composites extended NPK release up to several hours,<sup>89</sup> while a carboxymethyl cellulose system with varied fillers can extend release of NPK up to several days.<sup>79</sup> A mixture of maize starch and CNFs can release dimethyl phthalate, a model encapsulant, for up to a week.90 These examples indicate that the release profiles reported here are similar to other biocompatible, biopolymerbased systems.

The environmental impact of utilizing nanocellulose is difficult to quantify precisely, as life cycle analysis conclusions for these types of materials are highly dependent on the process and application.91 However, the process utilized here aims to minimize carbon emissions and energy consumption through optimizing the number of passes needed during the mechanical disintegration of the nanocellulose, which is the main source of energy consumption in this process.92 Likewise, by using nanocellulose as opposed to traditional sources, such as dissolving pulp, the bead formation process used herein does not necessitate pretreatment. This process is also not dependent on the raw material of choice, allowing for the use of side streams from other processes and the use of unbleached cellulose pulps containing other biopolymers such as hemicelluloses, lignin, and pectin.31 The biocompatibility, ability to use diverse feedstocks, improved release values, and versatility of this method to further optimize materials arguably outweigh concerns regarding the use of nanocellulose. This nanocellulose-based product is a promising material for EEF development with potential longterm benefits for agriculture and the environment.

Notable and unique benefits of the methodology described herein are the high loading of NPK and the tunable release. The latter is attainable by appropriately modulating the reaction time to create hydrophobic shells of varied thicknesses, with unique release profiles tuned for specific applications.<sup>93</sup> Due to this tunability, highly specified release profiles could be created by combining mixtures of hydrogels with varied degrees of esterification. As plant nutrient needs vary throughout the growth cycle,94 such systems could be envisioned to prevent the need for mid-season fertilization. Similarly, functionalization could be explored with other suitably volatile reagents with different levels hydrophobicity, enabling control of the release profile by varying the identity of the ester chain (see Fig. 1). Further, an additional degree of tunability in release kinetics has been demonstrated through modulating the loading percentage. Specifically, it has been shown that 36% loading of NPK provides a roughly three-fold decrease in release rates for gas

phase modified samples, an effect ascribed to the lower fraction of nutrients observed at the exposed surface of these beads.

More significantly, the results reported herein suggest a degree of tunability solely through modulating the extent of modification. Further, based on other reported results in the literature, it is likely that coupling of modification strategies can tune and extend release even further, to be competitive with current commercial products. For example, the esterification reactions which have proven effective at modifying release could be coupled with crosslinking and densification to further reduce the active hydrophilic hydroxyl sites in the beads.95 Alternatively, the esterified hydrophobic layer could then be sprayed with a thin layer of beeswax, which could lead to better adherence of the coating to the surface due to the similarities in hydrophobicity. 96,97 Utilizing multiple modification strategies at once also introduces multiple tunable variables, such as beeswax coating thickness or crosslinking extent, which should introduce finer control of nutrient release kinetics. These multiply-modified beads warrant further research.

# Conclusions

This work details a strategy of saturating nanocellulose-based hydrogel beads with a soluble NPK fertilizer, followed by a green gas-phase esterification strategy using hexanovl chloride. The initial loading of NPK within the hydrogel matrix was found to impact release kinetics due to loadingdependent differences in the fraction of nutrients at the surface as opposed to the interior of the beads. Additionally, controlled hydrophobization of the cellulose beads provided a route to slow and control the diffusion of nutrients out of the nanocellulose matrix by more than an order of magnitude by providing a hydrophobic barrier. While the release profiles obtained herein are not yet commercially competitive, performing the hydrophobic modification in the gas-phase allows for controllable modification of this material, eliminates the need for solvent, reduces energy inputs, and allows for surface-to-core modification of the hydrogel. Moreover, the cellulose utilized here was regenerated from agroforest byproducts, producing a circular economy of materials usage. Overall, this work proposes a sustainable biobased alternative to conventional EEFs, thereby improving crop yields while avoiding generation of secondary pollutants.

# **Author contributions**

DG-M: conceptualization, methodology, investigation, formal analysis, visualization, writing – original draft. SGP: conceptualization, methodology, investigation, formal analysis, visualization, writing – original draft. SV: methodology, investigation, writing – review and editing. PCB: conceptualization, methodology, investigation, analysis. JCW: methodology, supervision, resources, writing – review

and editing. DHF: conceptualization, methodology, supervision, resources, writing – review and editing. MSP: conceptualization, methodology, supervision, resources, project administration, funding acquisition, writing – review and editing.

# Conflicts of interest

The authors declare no conflict of interest.

# Acknowledgements

This work was supported by the USDA National Institute of Food and Agriculture, Hatch program (ALA013-17003) and McIntire-Stennis program (1022526). Contributions from SGP, JCW, and DHF were supported by the National Science Foundation under Grant No. CHE-2001611, the NSF Center for Sustainable Nanotechnology (CSN). The CSN is part of the NSF Centers for Chemical Innovation (CCI) Program. Contributions from SV were supported by a grant from USDA NIFA AFRI 2021-67021-34001. The authors thank Patrick Eckhert (Johns Hopkins University, Baltimore, MD) for performing SEM-EDS analysis.

# References

- 1 J. Chen, S. Lü, Z. Zhang, X. Zhao, X. Li, P. Ning and M. Liu, Environmentally friendly fertilizers: A review of materials used and their effects on the environment, *Sci. Total Environ.*, 2018, **613**, 829–839.
- X. Zhang, E. A. Davidson, D. L. Mauzerall, T. D. Searchinger,
   P. Dumas and Y. Shen, Managing nitrogen for sustainable development, *Nature*, 2015, 528, 51-59.
- 3 H. Guo, J. C. White, Z. Wang and B. Xing, Nano-enabled fertilizers to control the release and use efficiency of nutrients, *Curr. Opin. Environ. Sci. Health*, 2018, **6**, 77–83.
- 4 R. Prasad, Fertilizer urea, food security, health and the environment, *Curr. Sci.*, 1998, 75, 677–683.
- 5 G. Liu, L. Zotarelli, Y. Li, D. Dinkins, Q. Wang and M. Ozores-Hampton, Controlled-release and slow-release fertilizers as nutrient management tools, USA: US Department of Agriculture, UF/IFAS Extension Service, University of Florida, IFAS, 2014.
- 6 A. Shaviv and R. Mikkelsen, Controlled-release fertilizers to increase efficiency of nutrient use and minimize environmental degradation-A review, Fert. Res., 1993, 35, 1–12.
- 7 R. Prasad and Y. S. Shivay, Enhanced efficiency fertilizers or slow-release and NI/UI blended nitrogen fertilizers, *Indian J. Fert.*, 2021, 17, 316–321.
- 8 S. Shakiba, C. E. Astete, S. Paudel, C. M. Sabliov, D. F. Rodrigues and S. M. Louie, Emerging investigator series: polymeric nanocarriers for agricultural applications: synthesis, characterization, and environmental and biological interactions, *Environ. Sci.: Nano*, 2020, 7, 37–67.
- 9 P. P. Motavalli, K. W. Goyne and R. P. Udawatta, Environmental impacts of enhanced-efficiency nitrogen fertilizers, *Crop Management*, 2008, 7, 1–15.

- 10 B. Azeem, K. KuShaari, Z. B. Man, A. Basit and T. H. Thanh, Review on materials & methods to produce controlled release coated urea fertilizer, J. Controlled Release, 2014, 181, 11-21.
- 11 A. Alexander and H. U. Helm, Ureaform as a slow release fertilizer: a review, Z. Pflanzenernaehr. Bodenkd., 1990, 153, 249-255.
- 12 J. J. Perez and N. J. Francois, Chitosan-starch beads prepared by ionotropic gelation as potential matrices for controlled release of fertilizers, Carbohydr. Polym., 2016, 148, 134-142.
- 13 A. M. Smith and L. M. Gilbertson, Rational ligand design to improve agrochemical delivery efficiency and advance agriculture sustainability, ACS Sustainable Chem. Eng., 2018, 6, 13599-13610.
- 14 M. Y. Naz and S. A. Sulaiman, Slow release coating remedy for nitrogen loss from conventional urea: a review, J. Controlled Release, 2016, 225, 109-120.
- 15 K. Nelson, P. Scharf, L. Bundy and P. Tracy, Agricultural management of enhanced-efficiency fertilizers in the northcentral United States, Crop Management, 2008, 7, 1-12.
- 16 R. Tao, C. You, Q. Qu, X. Zhang, Y. Deng, W. Ma and C. Huang, Recent advances in the design of controlled-and sustained-release micro/nanocarriers of pesticide, Environ. Sci.: Nano, 2023, 351-371.
- 17 N. Katsumi, T. Kusube, S. Nagao and H. Okochi, The role of coated fertilizer used in paddy fields as a source of microplastics in the marine environment, Mar. Pollut. Bull., 2020, 161, 111727.
- 18 S. Piehl, A. Leibner, M. G. Löder, R. Dris, C. Bogner and C. Laforsch, Identification and quantification of macro-and microplastics on an agricultural farmland, Sci. Rep., 2018, 8, 17950.
- 19 FAO, World fertilizer outlook and trends to 2022, 2019.
- 20 A. Drescher, R. Glaser, C. Richert and K. Nippes, Demand for key nutrients (NPK) in the year 2050, Draft Report, University of Freiburg, Department of Geography, 2011, p. 77.
- 21 H. Teisala, M. Tuominen and J. Kuusipalo. Superhydrophobic Coatings on Cellulose-Based Materials: Fabrication, Properties, and Applications, Adv. Mater. Interfaces, 2014, 1, 1300026.
- 22 K. S. Kontturi, E. Kontturi and J. Laine, Specific water uptake of thin films from nanofibrillar cellulose, J. Mater. Chem. A, 2013, 1, 13655-13663.
- 23 A. Bashari, A. Rouhani Shirvan and M. Shakeri, Cellulosebased hydrogels for personal care products, Polym. Adv. Technol., 2018, 29, 2853-2867.
- 24 L.-Y. Long, Y.-X. Weng and Y.-Z. Wang, Cellulose Aerogels: Synthesis, Applications, and Prospects, Polymer, 2018, 10, 623.
- 25 H. Qi, R. Ma, C. Shi, Z. Huang, S. Liu, L. Sun and T. Hu, Novel low-cost carboxymethyl cellulose microspheres with excellent fertilizer absorbency and release behavior for saline-alkali soil, Int. J. Biol. Macromol., 2019, 131, 412-419.
- 26 A. Olad, H. Zebhi, D. Salari, A. Mirmohseni and A. R. Tabar, Slow-release NPK fertilizer encapsulated by carboxymethyl

- cellulose-based nanocomposite with the function of water retention in soil, Mater. Sci. Eng., C, 2018, 90, 333-340.
- 27 H. A. Essawy, M. B. Ghazy, F. Abd El-Hai and M. F. Superabsorbent hydrogels Mohamed, via graft polymerization of acrylic acid from chitosan-cellulose hybrid and their potential in controlled release of soil nutrients, Int. J. Biol. Macromol., 2016, 89, 144-151.
- 28 D. Franca, J. R. S. de Barros and R. Faez, Spray-dried cellulose nanofibrils microparticles as a vehicle for efficiency fertilizers, Cellulose, 2021, enhanced 1571-1585.
- 29 X. Luo and L. Zhang, Creation of regenerated cellulose microspheres with diameter ranging from micron to millimeter for chromatography applications, *I. Chromatogr.* A, 2010, 1217, 5922-5929.
- 30 J. Trygg, E. Yildir, R. Kolakovic, N. Sandler and P. Fardim, Anionic cellulose beads for drug encapsulation and release, Cellulose, 2014, 21, 1945-1955.
- 31 D. Gomez-Maldonado, S. Ponce and M. S. Peresin, The applicability of cellulose-Tara gum composite hydrogels as dye capture adsorbents, Water, Air, Soil Pollut., 2022, 233,
- 32 I. B. Vega Erramuspe, E. Fazeli, T. Näreoja, J. Trygg, P. Hanninen, T. Heinze and P. Fardim, Advanced cellulose efficient immobilization of for Biomacromolecules, 2016, 17, 3188-3197.
- 33 J. Trygg, E. Yildir, R. Kolakovic, N. Sandler and P. Fardim, Solid-State Properties and Controlled Release of Ranitidine Hydrochloride from Tailored Oxidised Cellulose Beads, Macromol. Mater. Eng., 2015, 300, 210-217.
- D. Gomez-Maldonado, I. Filpponen, L. S. Johansson, M. N. Waters, I. B. Vega Erramuspe and M. S. Peresin, Environmentally dependent adsorption of 2, 4-dichlorophenol on cellulose-chitosan self-assembled composites, Biopolymers, 2021, 112, e23434.
- 35 K. Gabov, T. Oja, T. Deguchi, A. Fallarero and P. Fardim, Preparation, characterization and antimicrobial application of hybrid cellulose-lignin beads, Cellulose, 2017, 24, 641-658.
- 36 B. Duan, X. Zheng, Z. Xia, X. Fan, L. Guo, J. Liu, Y. Wang, Q. Ye and L. Zhang, Highly biocompatible nanofibrous microspheres self-assembled from chitin in NaOH/urea aqueous solution as cell carriers, Angew. Chem., 2015, 127, 5241-5245.
- D. Gomez-Maldonado, I. Filpponen, J. A. Hernandez-Díaz, 37 M. N. Waters, M. L. Auad, L.-S. Johansson, I. B. Vega-Erramuspe and M. S. Peresin, Simple functionalization of cellulose beads with pre-propargylated chitosan for clickable scaffold substrates, Cellulose, 2021, 28, 6073-6087.
- 38 P. Trivedi, J. Trygg, T. Saloranta and P. Fardim, Synthesis of novel zwitterionic cellulose beads by oxidation and coupling chemistry in water, Cellulose, 2016, 23, 1751-1761.
- 39 J. Tang, J. Sisler, N. Grishkewich and K. C. Tam, Functionalization of cellulose nanocrystals for advanced applications, J. Colloid Interface Sci., 2017, 494, 397-409.
- 40 Y. Wang, H. Zhang, L. Lin, R. Wu, X. Wang, J. Ren, C. Liu and X. Wang, Modification of Cellulose by Hydrophobic

- Long-chain Molecules: Advances and Prospects, *Pap. Biomater.*, 2020, 5, 31–43.
- 41 C. Le Tien, M. Lacroix, P. Ispas-Szabo and M.-A. Mateescu, N-acylated chitosan: hydrophobic matrices for controlled drug release, *J. Controlled Release*, 2003, **93**, 1–13.
- 42 S. Milovanovic, D. Markovic, K. Aksentijevic, D. B. Stojanovic, J. Ivanovic and I. Zizovic, Application of cellulose acetate for controlled release of thymol, *Carbohydr. Polym.*, 2016, 147, 344–353.
- 43 D. Gomez-Maldonado, A. M. Reynolds, L.-S. Johansson, D. J. Burnett, J. B. Ramapuram, M. N. Waters, I. B. Vega Erramuspe and M. S. Peresin, Fabrication of aerogels from cellulose nanofibril grafted with β-cyclodextrin for capture of water pollutants, *J. Porous Mater.*, 2021, 28, 1725–1736.
- 44 G. K. Tripp, K. L. Good, M. J. Motta, P. H. Kass and C. J. Murphy, The effect of needle gauge, needle type, and needle orientation on the volume of a drop, *Vet. Ophthalmol.*, 2016, 19, 38–42.
- 45 M. S. Peresin, A. H. Vesterinen, Y. Habibi, L. S. Johansson, J. J. Pawlak, A. A. Nevzorov and O. J. Rojas, Crosslinked PVA nanofibers reinforced with cellulose nanocrystals: Water interactions and thermomechanical properties, *J. Appl. Polym. Sci.*, 2014, 131, 1–12.
- 46 B. P. Frank, C. Smith, E. R. Caudill, R. S. Lankone, K. Carlin, S. Benware, J. A. Pedersen and D. H. Fairbrother, Biodegradation of functionalized nanocellulose, *Environ. Sci. Technol.*, 2021, 55, 10744–10757.
- 47 C.-w. Du, J.-m. Zhou and A. Shaviv, Release characteristics of nutrients from polymer-coated compound controlled release fertilizers, *J. Polym. Environ.*, 2006, **14**, 223–230.
- 48 E. Motamedi, M. Safari and M. Salimi, Improvement of tomato yield and quality using slow release NPK fertilizers prepared by carnauba wax emulsion, starch-based latex and hydrogel nanocomposite combination, *Sci. Rep.*, 2023, 13, 11118.
- 49 R.-M. P. Karlsson, P. T. Larsson, P. Hansson and L. Wågberg, Thermodynamics of the water-retaining properties of cellulose-based networks, *Biomacromolecules*, 2019, 20, 1603–1612.
- 50 S. Lombardo and W. Thielemans, Thermodynamics of adsorption on nanocellulose surfaces, *Cellulose*, 2019, 26, 249–279.
- 51 C. Chang, B. Duan, J. Cai and L. Zhang, Superabsorbent hydrogels based on cellulose for smart swelling and controllable delivery, *Eur. Polym. J.*, 2010, **46**, 92–100.
- 52 R. Li, S. Wang, A. Lu and L. Zhang, Dissolution of cellulose from different sources in an NaOH/urea aqueous system at low temperature, *Cellulose*, 2015, 22, 339–349.
- 53 J. Grdadolnik and Y. Maréchal, Urea and urea-water solutions—an infrared study, *J. Mol. Struct.*, 2002, **615**, 177–189.
- 54 D. L. Freedman, J. M. Cashwell and B. J. Kim, Biotransformation of Explosive-Grade Nitrocellulose Under Nitrate-Reducing Conditions, *Proceedings of the Water Environment Federation*, 2000, vol. 2000(9), 200–210.

- 55 Y. Hosakun, K. Halász, M. Horváth, L. Csóka and V. Djoković, ATR-FTIR study of the interaction of CO2 with bacterial cellulose-based membranes, *Chem. Eng. J.*, 2017, 324, 83–92.
- 56 B. C. Beard, Cellulose nitrate as a binding energy reference in N (1s) XPS studies of nitrogen-containing organic molecules, *Appl. Surf. Sci.*, 1990, 45, 221–227.
- 57 N. Rehman, M. I. G. de Miranda, S. M. Rosa, D. M. Pimentel, S. M. Nachtigall and C. I. Bica, Cellulose and nanocellulose from maize straw: an insight on the crystal properties, *I. Polym. Environ.*, 2014, 22, 252–259.
- 58 K. A. Koivu, H. Sadeghifar, P. A. Nousiainen, D. S. Argyropoulos and J. Sipilä, Effect of fatty acid esterification on the thermal properties of softwood kraft lignin, ACS Sustainable Chem. Eng., 2016, 4, 5238–5247.
- 59 R. Pinton, N. Tomasi and L. Zanin, Molecular and physiological interactions of urea and nitrate uptake in plants, *Plant Signaling Behav.*, 2016, 11, e1076603.
- 60 N. Hue and J. Silva, Organic soil amendments for sustainable agriculture: organic sources of nitrogen, phosphorus, and potassium, *Plant nutrient management in Hawaii's soils, approaches for tropical and subtropical agriculture*, College of Tropical Agriculture and Human Resources, University of Hawaii, Manoa, 2000, pp. 133–144.
- 61 D. Paredes, C. Ortiz and R. Torres, Synthesis, characterization, and evaluation of antibacterial effect of Ag nanoparticles against Escherichia coli O157: H7 and methicillin-resistant Staphylococcus aureus (MRSA), *Int. J. Nanomed.*, 2014, 1717–1729.
- 62 F. Azzam, L. Heux, J.-L. Putaux and B. Jean, Preparation by grafting onto, characterization, and properties of thermally responsive polymer-decorated cellulose nanocrystals, *Biomacromolecules*, 2010, **11**, 3652–3659.
- 63 M. V. Biyani, E. J. Foster and C. Weder, Light-healable supramolecular nanocomposites based on modified cellulose nanocrystals, ACS Macro Lett., 2013, 2, 236–240.
- 64 R. Dash, T. Elder and A. J. Ragauskas, Grafting of model primary amine compounds to cellulose nanowhiskers through periodate oxidation, *Cellulose*, 2012, 19, 2069–2079.
- 65 E. Espino-Pérez, S. Domenek, N. Belgacem, C. Sillard and J. Bras, Green process for chemical functionalization of nanocellulose with carboxylic acids, *Biomacromolecules*, 2014, 15, 4551–4560.
- 66 M. Hasani, E. D. Cranston, G. Westman and D. G. Gray, Cationic surface functionalization of cellulose nanocrystals, *Soft Matter*, 2008, 4, 2238–2244.
- 67 M. Fumagalli, D. Ouhab, S. M. Boisseau and L. Heux, Versatile gas-phase reactions for surface to bulk esterification of cellulose microfibrils aerogels, *Biomacromolecules*, 2013, 14, 3246–3255.
- 68 G. David, N. Gontard, D. Guérin, L. Heux, J. Lecomte, S. Molina-Boisseau and H. Angellier-Coussy, Exploring the potential of gas-phase esterification to hydrophobize the surface of micrometric cellulose particles, *Eur. Polym. J.*, 2019, **115**, 138–146.

- 69 D. Bamberger, D. Hobernik, M. Konhäuser, M. Bros and P. R. Wich, Surface modification of polysaccharide-based nanoparticles with PEG and dextran and the effects on immune cell binding and stimulatory characteristics, *Mol. Pharmaceutics*, 2017, 14, 4403–4416.
- 70 K. Hua, E. Ålander, T. Lindström, A. Mihranyan, M. Strømme and N. Ferraz, Surface chemistry of nanocellulose fibers directs monocyte/macrophage response, *Biomacromolecules*, 2015, 16, 2787–2795.
- 71 M.-C. Jones, S. A. Jones, Y. Riffo-Vasquez, D. Spina, E. Hoffman, A. Morgan, A. Patel, C. Page, B. Forbes and L. A. Dailey, Quantitative assessment of nanoparticle surface hydrophobicity and its influence on pulmonary biocompatibility, *J. Controlled Release*, 2014, **183**, 94–104.
- 72 F. Rancan, Q. Gao, C. Graf, S. Troppens, S. Hadam, S. Hackbarth, C. Kembuan, U. Blume-Peytavi, E. Rühl and J. R. Lademann, Skin penetration and cellular uptake of amorphous silica nanoparticles with variable size, surface functionalization, and colloidal stability, ACS Nano, 2012, 6, 6829–6842.
- 73 J. M. Chan, L. Zhang, K. P. Yuet, G. Liao, J.-W. Rhee, R. Langer and O. C. Farokhzad, PLGA-lecithin-PEG core-shell nanoparticles for controlled drug delivery, *Biomaterials*, 2009, 30, 1627–1634.
- 74 D. He, S. Wang, L. Lei, Z. Hou, P. Shang, X. He and H. Nie, Core-shell particles for controllable release of drug, *Chem. Eng. Sci.*, 2015, 125, 108–120.
- 75 M. Leonardi, G. M. Caruso, S. C. Carroccio, S. Boninelli, G. Curcuruto, M. Zimbone, M. Allegra, B. Torrisi, F. Ferlito and M. Miritello, Smart nanocomposites of chitosan/alginate nanoparticles loaded with copper oxide as alternative nanofertilizers, *Environ. Sci.: Nano*, 2021, 8, 174–187.
- 76 P. Khanjani, A. W. King, G. J. Partl, L.-S. Johansson, M. A. Kostiainen and R. H. Ras, Superhydrophobic paper from nanostructured fluorinated cellulose esters, ACS Appl. Mater. Interfaces, 2018, 10, 11280–11288.
- 77 S. Guzman-Puyol, G. Tedeschi, L. Goldoni, J. J. Benítez, L. Ceseracciu, A. Koschella, T. Heinze, A. Athanassiou and J. A. Heredia-Guerrero, Greaseproof, hydrophobic, and biodegradable food packaging bioplastics from C6-fluorinated cellulose esters, *Food Hydrocolloids*, 2022, 128, 107562.
- 78 G. Rozo, L. Bohorques and J. Santamaría, Controlled release fertilizer encapsulated by a κ-carrageenan hydrogel, *Polímeros*, 2019, 29, e2019033.
- 79 C. R. Bauli, G. F. Lima, A. G. de Souza, R. R. Ferreira and D. S. Rosa, Eco-friendly carboxymethyl cellulose hydrogels filled with nanocellulose or nanoclays for agriculture applications as soil conditioning and nutrient carrier and their impact on cucumber growing, *Colloids Surf.*, A, 2021, 623, 126771.
- 80 R. K. Owusu, Q. Zhu and E. Dickinson, Controlled release of L-tryptophan and vitamin B2 from model water/oil/water multiple emulsions, *Food Hydrocolloids*, 1992, **6**, 443–453.

- 81 S. A. Bravo, M. C. Lamas and C. J. Salomón, In-vitro studies of diclofenac sodium controlled-release from biopolymeric hydrophilic matrices, *J. Pharm. Pharm. Sci.*, 2002, 5, 213–219.
- 82 I. Smirnova, S. Suttiruengwong and W. Arlt, Feasibility study of hydrophilic and hydrophobic silica aerogels as drug delivery systems, *I. Non-Cryst. Solids*, 2004, **350**, 54–60.
- 83 N. Ganonyan, G. Bar, R. Gvishi and D. Avnir, Gradual hydrophobization of silica aerogel for controlled drug release, *RSC Adv.*, 2021, **11**, 7824–7838.
- 84 T. Pellegrino, L. Manna, S. Kudera, T. Liedl, D. Koktysh, A. L. Rogach, S. Keller, J. Rädler, G. Natile and W. J. Parak, Hydrophobic nanocrystals coated with an amphiphilic polymer shell: a general route to water soluble nanocrystals, *Nano Lett.*, 2004, 4, 703–707.
- 85 Y. Miyako, N. Khalef, K. Matsuzaki and R. Pinal, Solubility enhancement of hydrophobic compounds by cosolvents: role of solute hydrophobicity on the solubilization effect, *Int. J. Pharm.*, 2010, **393**, 48–54.
- 86 F. Najafi, M. Salami-Kalajahi and H. Roghani-Mamaqani, Synthesis of amphiphilic Janus dendrimer and its application in improvement of hydrophobic drugs solubility in aqueous media, *Eur. Polym. J.*, 2020, 134, 109804.
- 87 M. Fumagalli, F. Sanchez, S. M. Boisseau and L. Heux, Gasphase esterification of cellulose nanocrystal aerogels for colloidal dispersion in apolar solvents, *Soft Matter*, 2013, 9, 11309–11317.
- 88 A. Jarosiewicz and M. Tomaszewska, Controlled-release NPK fertilizer encapsulated by polymeric membranes, *J. Agric. Food Chem.*, 2003, 51, 413–417.
- 89 L. L. Messa and R. Faez, Spray-dried chitosan/nanocellulose microparticles: synergistic effects for the sustained release of NPK fertilizer, *Cellulose*, 2020, 27, 10077–10093.
- 90 M. D. Patil, V. D. Patil, A. A. Sapre, T. S. Ambone, A. A. T. Torris, P. G. Shukla and K. Shanmuganathan, Tuning controlled release behavior of starch granules using nanofibrillated cellulose derived from waste sugarcane bagasse, ACS Sustainable Chem. Eng., 2018, 6, 9208–9217.
- 91 F. Foroughi, E. Rezvani Ghomi, F. Morshedi Dehaghi, R. Borayek and S. Ramakrishna, A Review on the Life Cycle Assessment of Cellulose: From Properties to the Potential of Making It a Low Carbon Material, *Materials*, 2021, 14, 714.
- 92 L. C. Malucelli, M. Matos, C. Jordão, D. Lomonaco, L. G. Lacerda, M. A. S. Carvalho Filho and W. L. E. Magalhães, Influence of cellulose chemical pretreatment on energy consumption and viscosity of produced cellulose nanofibers (CNF) and mechanical properties of nanopaper, *Cellulose*, 2019, 26, 1667–1681.
- 93 W. Liu, W. D. Wu, C. Selomulya and X. D. Chen, Facile spray-drying assembly of uniform microencapsulates with tunable core-shell structures and controlled release properties, *Langmuir*, 2011, 27, 12910–12915.
- 94 J. Y. Lee, A. Rahman, H. Azam, H. S. Kim and M. J. Kwon, Characterizing nutrient uptake kinetics for efficient crop production during Solanum lycopersicum var. cerasiforme

- Alef. growth in a closed indoor hydroponic system, *PLoS One*, 2017, 12, e0177041.
- 95 Y. L. Lee, O. H. Ahmed, S. A. Wahid, M. B. Jalloh and A. A. Muzah, Nutrient release and ammonia volatilization from biochar-blended fertilizer with and without densification, *Agronomy*, 2021, **11**, 2082.
- 96 Y. Huang, Q. Hu, G. Cui, X. Guo, B. Wei, C. Gan, W. Li, D. Mo, R. Lu and J. Cui, Release-controlled microcapsules of
- thiamethoxam encapsulated in beeswax and their application in field, *J. Environ. Sci. Health, Part B*, 2020, 55, 342–354.
- 97 P. Boonying, K. Boonpavanitchakul and W. Kangwansupamonkon, Green Bio-composite Coating Film from Lignin/Pre-vulcanized Natural Rubber Latex for Controlled-release Urea Fertilizer, *J. Polym. Environ.*, 2023, 31, 1642–1655.